coatings

MDPI

*Article*

# Effects of Mixed Microcapsules in Different Proportions on Aging Resistance and Self-Healing Properties of Waterborne Coatings for *Tilia europaea* L.

**Lingran Xia [1,2], Yan Han [1,2], Taiyu Yin [1,2], Ye Zhu [1,2], Xiaoxing Yan [1,2,*] and Jun Li [1,2]**

[1] Co-Innovation Center of Efficient Processing and Utilization of Forest Resources, Nanjing Forestry University, Nanjing 210037, China; xialingran@njfu.edu.cn (L.X.); hanyan@njfu.edu.cn (Y.H.); yintaiyu@njfu.edu.cn (T.Y.); zhuye@njfu.edu.cn (Y.Z.); lijun0099@njfu.edu.cn (J.L.)

[2] College of Furnishings and Industrial Design, Nanjing Forestry University, Nanjing 210037, China

* Correspondence: yanxiaoxing@njfu.edu.cn

**Abstract:** In order to prolong the effective time of the self-healing properties of waterborne coatings containing shellac microcapsules coated with melamine rice husk powder (MRHP), three kinds of MRHPs with better microscopic morphologies, which contain 2.8% (type A), 5.5% (type B), and 8.0% (type C) of a rice husk powder (RHP), in shell materials were mixed according to three different proportions, and added to the waterborne coatings based on *Tilia europaea* L., under the conditions of the most proper addition amount of 6.0% microcapsules. The results indicated that the waterborne coatings containing mixed microcapsules can still maintain the best state in terms of optical properties and mechanical properties, with a chromatism of 1.10, an adhesion of zero, a hardness of 4H, an impact resistance of 7 kg·cm, and an elongation at break of 35.28%, respectively. According to the aging resistance test, the waterborne coating containing microcapsules "type A + type B + type C" demonstrated a longer effective time. After aging for 200 h in the UV climate resistance test chamber, the light loss rate at an incident angle of 60° was 2.91%. Through scratch testing, it is verified that the mixed microcapsules can prolong the self-healing time, reduce the crack size, and achieve a coating self-healing rate of 41.11%. They can also inhibit the crack growth rate to a certain extent. Roughness tests indicated that the surface roughness of the coating with mixed microcapsules increased by 0.038 μm in comparation with the single microcapsule, but the surface can still remain smooth after being covered by the topcoat without the microcapsules. Studying the ratio of mixed microcapsules provides new ideas for the optimization of a wood-based coating self-healing effect.

**Keywords:** microcapsule; waterborne coating; self-healing; aging resistance; mixing ratio



**Citation:** Xia, L.; Han, Y.; Yin, T.; Zhu, Y.; Yan, X.; Li, J. Effects of Mixed Microcapsules in Different Proportions on Aging Resistance and Self-Healing Properties of Waterborne Coatings for *Tilia europaea* L. *Coatings* **2024**, *14*, 1042. https://doi.org/10.3390/coatings14081042

Academic Editor: Flavio Deflorian

Received: 15 July 2024
Revised: 12 August 2024
Accepted: 13 August 2024
Published: 15 August 2024



## 1. Introduction

With the development of society, the furniture industry is moving towards a green, sustainable, and material-saving direction [1–3]. Wood, due to its renewable, recyclable, and naturally degradable green properties [4–6], is widely used in fields such as building structures, furniture manufacturing, and papermaking [7–11]. However, wood has the characteristic of drying shrinkage and wet expansion, and is prone to a cracking under changes in environmental factors [12]. Typically, to extend the lifespan of wood products, a coating is applied to the surface to shield it from external air, moisture, and other substances for its protection [13,14]. The waterborne coating, which is environmentally and human-health friendly, can protect wooden materials to a certain extent [15,16]. Using water as a solvent enables a significant reduction in the usage of organic solvents [17,18]. The evaporation of organic solvents leads to air pollution and poses a fire hazard. Waterborne coatings, however, can mitigate these issues [19]. However, the waterborne coatings on wood surfaces are notoriously limited in terms of mechanical properties compared with traditional coatings [20]. With a positive response and the implementation of environmental

policies in the furniture industry, waterborne wood coatings have gradually replaced traditional wood coatings. Their application has become increasingly widespread within the industry [21–23]. Therefore, it is necessary to explore new ways to optimize waterborne wood coatings.

Microcapsules with a self-healing function have been widely used in the field of coatings. Li et al. [24] prepared poly(urea-formaldehyde) shell-coated tung oil microcapsules via an in situ polymerization and added an epoxy resin to prepare a dual-functional coating with self-healing and self-lubricating functions, which was suitable for metal surfaces. Song et al. [25] synthesized isoflurane diisocyanate microcapsules with a polyurethane/poly(urea-formaldehyde) double-shell structure by interfacial polymerization and in situ polymerization. The coating incorporating the microcapsules demonstrated an excellent self-healing effect and corrosion resistance in the artificial scratch area. Tezel et al. [26] added epoxy microcapsules coated with poly(urea-formaldehyde) and polyethyleneimine microcapsules coated with poly(melamine-urea-formaldehyde) to epoxy–polyester acrylate resin to prepare a self-healing coating applied to the surface of plexiglass, and, after two days, the artificial scratches were successfully repaired. Uzoma et al. [27] used a mixture of fluorocarbon resin and urea–formaldehyde resin to coat fluorosilane via interfacial polymerization to prepare a multi-stimulus wettability response coating, and the coating achieved good hydrophobic and self-healing properties. The existing studies on the use of microcapsules to improve the self-healing properties of coatings mainly focus on the repair of coatings with metal and glass substrates. However, the utilization of microcapsules in waterborne coatings for the wood industry is still in the exploratory stage.

Shellac, a natural material [28], is commonly used in the resurfacing of wooden furniture [29]. Dissolving shellac in ethanol as a core material solution allows for physical curing at room temperature, effectively filling microcracks in acrylic resin. Melamine resin is often used as a shell material for microcapsules [30]. On the other hand, the triazine ring structure in the melamine resin also produces the disadvantages of insufficient toughness and high brittleness [31]. Rice husk powder (RHP) is mainly composed of cellulose, which is an environmentally friendly material with a low price, easy availability, and good toughness [32,33]. The waterborne coating added with microcapsules of shellac as the core material coated with melamine rice husk powder (MRHP) has a good self-healing ability after being damaged by mechanical forces, high temperature, and ultraviolet light [34]. However, with a single proportion of RHP, the self-healing function can only take effect for a short time. It may be improved by adding the different mixed kinds of microcapsules. Therefore, this paper studies the optimal addition ratio of microcapsules with different RHP contents for the aging resistance and self-healing properties of waterborne coatings.

Preliminary research results [35–37] showed that the optimal coating process of waterborne coatings on the Basswood surface is “three times of primer, two times of topcoat, adding 6.0% microcapsules to the primer”, and the optimal content of RHP is 5.5%. In this paper, the microcapsules with 2.8% and 8.0% RHP in the shell material and the microcapsules with the optimal 5.5% RHP in the shell material were mixed in different proportions. Then, the different types of mixed microcapsules were added to the waterborne coating, and then applied to the Basswood board by the optimal coating process. To explore the effect of different types of mixed microcapsules, the optical properties, mechanical properties, micromorphology, and chemical composition of the waterborne coatings were examined. Aging resistance tests were carried out on waterborne coatings containing different types of mixed microcapsules and a single microcapsule with the optimum content of RHP. The findings of the research offer a solid technological foundation for the preparation of self-healing microcapsules and self-healing coatings.

## 2. Experimental Section

### *2.1. Materials*

The 37.0% formaldehyde solution ($M_w$: 30.03 g/mol, CAS No.: 50-00-0) was purchased from Chengdu Minsheng Disinfectant Co., Ltd., Chengdu, China. Melamine

($M_w$: 60.06 g/mol, CAS No.: 57-13-6) was purchased from Sinopharm Chemical Reagent Co., Ltd., Shanghai, China. Triethanolamine ($M_w$: 149.18 g/mol, CAS No.: 102-71-6), sodium dodecylbenzene sulfonate ($M_w$: 348.48 g/mol, CAS No.: 25155-30-0), and citric acid monohydrate ($M_w$: 210.14 g/mol, CAS No.: 5949-29-1) were obtained from Xilong Science Co., Ltd., Shantou, China. The RHP (100 mesh) was provided by Beijing Huajieqitai Trading Co., Ltd., Beijing, China, which was ground by a powder machine. Shellac was obtained from Shuangjiang Yuye Forest Chemical Products Co., Ltd., Lincang, China, which was the Yunnan special grade II. *Tilia europaea* L. (Basswood, 100 mm × 65 mm × 4 mm) was provided by Yunhe Youlin Wood Industry Co., Ltd., Lishui, China. Glass plates (75 mm × 25 mm) were obtained from Jiangsu Feizhou glass plastic Co., Ltd., Yancheng, China. Waterborne primer and finishing (waterborne acrylic copolymer dispersion, matting agent, additives, and water, 30.0% solid content) were provided by Changsha Haodu Coatings Co., Ltd., Changsha, China. Absolute ethanol (99.5%, $M_w$: 46.07 g/mol, CAS No.: 64-17-5) was offered by Taicang Xintai Alcohol Co., Ltd., Suzhou, China.

### 2.2. Methods

(1) Preparation of melamine/RHP-coated shellac microcapsules

According to References [35,38], the microcapsules with an RHP content of 2.8% (type A), 5.5% (type B), and 8.0% (type C) were prepared, using the melamine resin with the added RHP as a shell material and the shellac solution as a core material. Table 1 provides a detailed list of the experimental raw material consumption.

**Table 1.** Detailed list of the experimental raw material consumption.

| Type | RHP Content (%) | RHP (g) | Melamine (g) | 37% Formaldehyde Solution (g) | Shellac (g) |
|---|---|---|---|---|---|
| A | 2.8 | 0.25 | 5.00 | 10.00 | 6.64 |
| B | 5.5 | 0.50 | 5.00 | 10.00 | 6.83 |
| C | 8.0 | 0.75 | 5.00 | 10.00 | 7.01 |

(2) Preparation of self-healing waterborne coating

The ratios of different kinds of mixed microcapsules and the ingredients of waterborne coatings are summarized in Table 2. The process of the waterborne coating was "three times primer, two times topcoat, 6.0% microcapsules added in the primer". Take sample 1# as an example. After mixing the type A and type B microcapsules at a mass ratio of 1:1 evenly, the 0.12 g of mixed microcapsules were weighed and added to 1.88 g of waterborne primer. After stirring evenly, the waterborne primer containing 6.0% microcapsules was prepared successfully. The 2.0 g of waterborne finishing was weighed for use. An appropriate amount of primer was weighed with a special brush and applied evenly on the polished Basswood board surface. Then, it was dried for 4 h in a cool and ventilated place. After gently sanding the surface with 600-grit sandpaper, the debris was swept away with a clean brush. The operation of the primer painting was repeated twice. Similarly, the finishing was also applied twice, as described above. Finally, the coated Basswood board was dried at room temperature for 24 h. Samples 2#–6# were all painted according to the same procedure.

**Table 2.** Ratio of different kinds of mixed microcapsules and waterborne coating components.

| Coating Number (#) | Kind of Mixed Microcapsules | Mixing Ratio (%) | Mass of Microcapsules (g) | Mass of Primer (g) | Mass of Finish (g) | Mass of Waterborne Coatings (g) |
|---|---|---|---|---|---|---|
| 1 | type A + type B | 1:1 | 0.12 | 1.88 | 2.00 | 4.00 |
| 2 | type B + type C | 1:1 | 0.12 | 1.88 | 2.00 | 4.00 |
| 3 | type A + type B + type C | 1:1:1 | 0.12 | 1.88 | 2.00 | 4.00 |
| 4 | type A | 1 | 0.12 | 1.88 | 2.00 | 4.00 |
| 5 | type B | 1 | 0.12 | 1.88 | 2.00 | 4.00 |
| 6 | type C | 1 | 0.12 | 1.88 | 2.00 | 4.00 |

### 2.3. Testing and Characterization

The HP-2136 chromatism meter (Shenzhen Threenh Technology Co., Ltd., Shenzhen, China) was used to test the chromatism of the coating. $L$ stands for lightness, $a$ stands for the red–green phase, and $b$ stands for the yellow–blue phase. For the chromatism test, a point on the coating was randomly selected and tested to obtain the values of $L_1$, $a_1$, and $b_1$. Similarly, another point was tested to obtain the values of $L_2$, $a_2$, and $b_2$. According to Formula (1), $\Delta L = L_1 - L_2$ (lightness difference), $\Delta a = a_1 - a_2$ (red/green difference), $\Delta b = b_1 - b_2$ (yellow/blue difference), the chromatism $\Delta E$ was calculated as follows:

$$\Delta E = [(\Delta L)^2 + (\Delta a)^2 + (\Delta b)^2]^{1/2} \quad (1)$$

The HG268 intelligent gloss meter (Shenzhen Threenh Technology Co., Ltd., Shenzhen, China) was used to test the gloss of the coating. According to GB/T 4893.6-2013 [39], the gloss with three incidences of 20°, 60°, and 85° was recorded, respectively. A pencil hardness tester (Cangzhou Jieke Instrument and Equipment Manufacturing Co., Ltd., Cangzhou, China) was used to test the surface hardness of the paint film according to GB/T 6739-2022 [40], while the QFH-HG600 coating film cross-cutting tester (Cangzhou Jinghong Engineering Instrument Co., Ltd., Cangzhou, China) was used for testing the coating adhesion according to GB/T 4893.4-2013 [41]. With a cutting tool, a grid was formed on the coating and covered with tape. The tape was removed after 5 min. The adhesion level of coating was determined according to the peeling situation of the coating on the tape. The coating adhesion had 1–5 levels, and the samples in this study showed the best level 1. According to GB/T 1732-2020 [42], the QCJ coating impact tester (Jinan Ruima Testing Machine Manufacturing Co., Ltd., Jinan, China) was used to test the impact resistance of the coating. The minimum height of the steel ball until the coating was damaged was recorded as the impact strength of the paint film. A universal testing machine (Xieqiang Instrument Manufacturing Co., Ltd., Shanghai, China) was used to determine an elongation at break ($E$) according to the standard BS EN 15977-2011 [43]. The result was calculated according to Formula (2), where $L0$ is the original marking distance of the sample, mm; $L$ is the marking distance when the sample was fractured, mm, as follows:

$$E = \frac{(L - L0)}{L0} \times 100\% \quad (2)$$

A Quanta-200 scanning electron microscope (SEM, FEI Co., Ltd., Hillsboro, OR, USA) was used to observe the microscopic morphology of the microcapsules and coatings. A VERTEX 80V infrared spectrum analyzer (Germany Bruker Co., Ltd., Karlsruhe, Germany) was used to analyze the chemical composition of the microcapsules and coatings.

The different samples were put into a 120 °C oven, a 160 °C oven, and an ultraviolet (UV) weathering test chamber (Dongguan Jiedong Experimental Equipment Co., Ltd., Dongguan, China), respectively, to conduct an aging test on the coatings. The sample was put in the oven, and the chromatism and gloss of the coatings were tested every 8 h for a total of 40 h. The samples were placed in the UV weathering test chamber, tested every 40 h, and the change in the chromatism and gloss of the coatings was recorded for a total of 200 h. The UV region was considered as 290–400 nm, and the illumination level was 0.08 W/cm$^2$. The distance of the light source from the surface of the coatings was about 15 cm. One important evaluation method for detecting the degree of aging during coating aging is the light loss rate (LLR). The 60° gloss was measured by the HG268 intelligent gloss meter. As shown in Formula (3), $A$ and $B$ represent the measured values of gloss before and after aging, and LLR was calculated as follows:

$$G = \frac{(A - B)}{A} \times 100\% \quad (3)$$

In the scratch test, in order to observe the scratch morphology and the self-healing effect of the waterborne coating more intuitively, the same coating process was used to

evenly coat the waterborne coating on the surface of the glass plate. After drying at room temperature, the coating was scratched with a thin blade. The scratch changes at 1 d, 3 d, 7 d, and 14 d were observed by a Zeiss Axio scope A1 biological microscope (OM, Zeiss Optical Instruments International Trade Co., Ltd., Shanghai, China). According to Formula (4), the self-healing rate of the paint film was calculated. $W_b$ is the initial width of the widest scratch, mm; $W_a$ is the width of the scratch at the same position after healing, mm, as follows:

$$W = \frac{(W_b - W_a)}{W_b} \times 100\% \quad (4)$$

The roughness was measured using the fine roughness tester JB-4C (Shanghai Shunyu Hengping Scientific Instrument Co., Ltd., Shanghai, China).

All experiments were repeated 4 times with an error which was less than 5.0%.

## 3. Results and Discussion

### *3.1. Morphology and Chemical Composition Analysis of Microcapsules with Different Contents of RHP*

#### 3.1.1. Morphology Characterization of Microcapsules

The surface morphology of microcapsules with different contents of RHP is shown in Figure 1. The microcapsules with RHP added to the shell material had uniform particle sizes and good microcapsule morphologies. Figure 2 shows the particle sizes of the microcapsules with different contents of RHP. Figure 2A–C illustrate the particle sizes of the type A, type B, and type C microcapsules, respectively. Among them, the type B microcapsule demonstrated uniform particle sizes for about 0–5 μm, with the shape of round and uniform spheres. Meanwhile, the type A and type C microcapsules also had similar morphologies, with particle sizes of 0–5 μm, and showed no agglomeration.

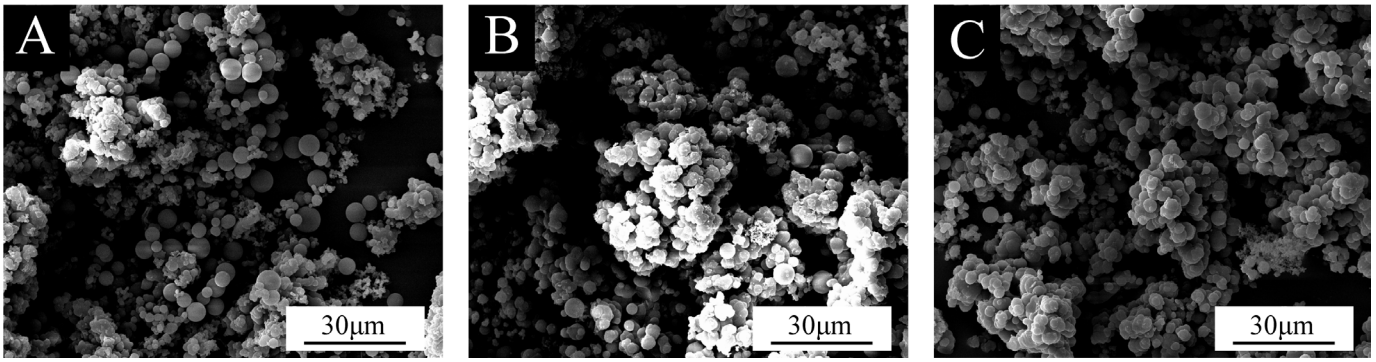


**Figure 1.** SEM images of microcapsules with different RHP contents: (**A**) 2.8%, (**B**) 5.5%, and (**C**) 8.0%.

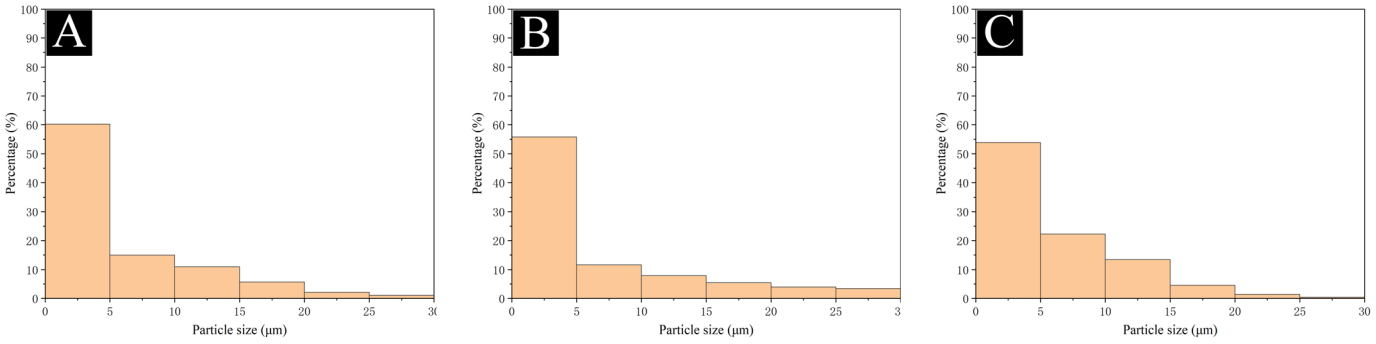


**Figure 2.** Particle sizes of different types of microcapsules: (**A**) 2.8%, (**B**) 5.5%, and (**C**) 8.0%.

3.1.2. Infrared Spectra Testing

Figure 3 shows the infrared spectra of four types of microcapsules. The absorption peak at 1547 $cm^{-1}$ was the stretching vibration of -NH- and belonged to the characteristic peak of the melamine resin. The infrared spectrum of the microcapsule with RHP added to the shell material had a peak change at 1157 $cm^{-1}$. It can be speculated that this peak was affected by the C-H vibration of the aromatic core of lignin in the RHP and the antisymmetric stretching vibration peak of the C-O-C bridge bond, implying that the shell material of the microcapsule contains RHP. The absorption peaks of the infrared spectra at other positions of the microcapsules were consistent with those of the type A microcapsule, that is, the chemical composition of the microcapsules did not change.

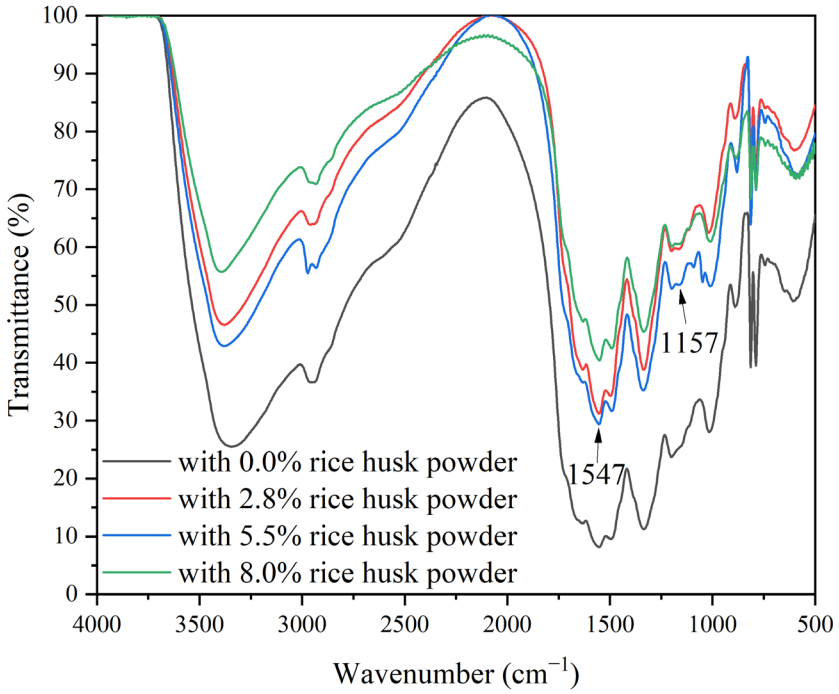


**Figure 3.** Infrared spectrum of different types of microcapsules.

*3.2. Optical and Mechanical Properties Analysis*

3.2.1. Chromatism

Table 3 shows the effect of mixed microcapsules in different proportions on the chromatism of the waterborne coatings. There was no significant difference in the effect of the mixed microcapsules in different proportions on the chromatism of the waterborne coatings because of the same coating process and similar morphologies of the microcapsules.

**Table 3.** Effect of mixed microcapsules in different proportions on the chromatism of waterborne coatings.

| Sample Number (#) | $L_1$ | $a_1$ | $b_1$ | $L_2$ | $a_2$ | $b_2$ | $\Delta L$ | $\Delta a$ | $\Delta b$ | $\Delta E$ |
|---|---|---|---|---|---|---|---|---|---|---|
| 1 | 72.0 | 12.4 | 23.3 | 71.5 | 13.9 | 23.9 | −0.5 | 1.5 | 0.6 | 1.69 |
| 2 | 70.3 | 13.3 | 31.0 | 70.6 | 12.5 | 29.8 | 0.3 | −0.8 | −1.2 | 1.47 |
| 3 | 70.8 | 13.8 | 27.7 | 70.6 | 14.2 | 28.7 | −0.2 | 0.4 | 1.0 | 1.10 |
| 4 | 73.8 | 13.4 | 30.6 | 72.2 | 13.6 | 31.1 | −1.6 | 0.2 | 0.5 | 1.69 |
| 5 | 67.2 | 15.0 | 28.2 | 67.8 | 15.3 | 28.8 | 0.6 | 0.3 | 0.6 | 0.90 |
| 6 | 68.5 | 15.8 | 32.0 | 69.1 | 15.2 | 30.8 | 0.6 | −0.6 | −1.2 | 1.47 |

3.2.2. Gloss

The gloss data are summarized in Table 4. From Table 4, the data show that the gloss difference in samples 1#–5# is small, while sample 6#, which only contains the type C

microcapsule, has a lower gloss. The reason for this is considered to be that the cellulose distributed in the shell material of the microcapsules becomes non-uniform due to the high content of cellulose powder, which makes it easier to agglomerate. Therefore, the microcapsule type C is more likely to form into one cluster in the waterborne coating, resulting in a decrease in the coating gloss. However, since it is added to the primer, it has less effect on the overall coating.

**Table 4.** Effect of mixed microcapsules in different proportions on the gloss of waterborne coatings.

| Sample Number (#) | Gloss at the Incident Angle of 20° (%) | Gloss at the Incident Angle of 60° (%) | Gloss at the Incident Angle of 85° (%) |
|---|---|---|---|
| 1 | 12.3 | 32.7 | 37.5 |
| 2 | 11.1 | 29.8 | 35.1 |
| 3 | 16.8 | 40.0 | 48.8 |
| 4 | 14.5 | 40.6 | 46.1 |
| 5 | 19.3 | 43.0 | 55.4 |
| 6 | 8.3 | 27.8 | 29.4 |

#### 3.2.3. Mechanical Properties

Table 5 shows the hardness, adhesion, impact resistance, and elongation at break of waterborne coatings with mixed microcapsules in different proportions. The difference in adhesion and hardness between all samples was not significant because the microcapsules were added to the primer of the waterborne coatings, and their adhesion and hardness were mainly affected by the performance of the topcoat [44,45]. It was also shown that the impact resistance was improved as the content of RHP in the microcapsules increased. Among the samples 1#–3#, with microcapsules of "type B + type C", the coating achieved a better impact resistance than the others. However, all of the waterborne coatings containing microcapsules of type A, such as samples 1#, 3#, and 4#, performed deficiently on the impact resistance. For all of the samples, the elongation at break differed slightly. The toughness of sample 3# was the best. It can be inferred that the mixed microcapsules increase the toughness of the coating. In summary, the coating containing the mixed microcapsules "type A + type B + type C", which was sample 3#, was the best on the comprehensive mechanical properties.

**Table 5.** Effect of mixed microcapsules in different proportions on the mechanical properties of waterborne coatings.

| Sample Number (#) | Adhesion | Hardness | Impact Resistance (kg·cm) | Elongation at Break (%) |
|---|---|---|---|---|
| 1 | 0 | 4 H | 5 | 33.71 |
| 2 | 0 | 4 H | 10 | 26.05 |
| 3 | 0 | 4 H | 7 | 35.28 |
| 4 | 0 | 4 H | 5 | 28.62 |
| 5 | 0 | 4 H | 10 | 30.90 |
| 6 | 0 | 4 H | 10 | 23.59 |

#### 3.2.4. Microstructure

It can be seen from the above results that, among all of the samples, there is no obvious difference in the optical properties between samples 1# and 3#, with mixed microcapsules, and sample 5#, containing RHP microcapsules, as well as the mechanical properties. Figure 4 shows the micromorphology of all of the coating samples observed by the SEM. The results showed that samples 1#, 3#, 4#, and 5# were relatively smooth, while the coating surfaces of samples 2# and 6# had obvious protrusions, and there were a few bubbles in the coating of sample 6#. The reason may be due to the uneven distribution of the cellulose powder that caused caking with the high concentration of cellulose powder in the microcapsule shell increase. Therefore, the coating surface containing microcapsules of type C showed obvious protrusions. For sample 2#, the proportion of microcapsules of type C was large, and there were a few protrusions on the surface. The micromorphology

of the coating surface of samples 1# and 3# containing mixed microcapsules was as good as that of the coatings containing microcapsules of type B.

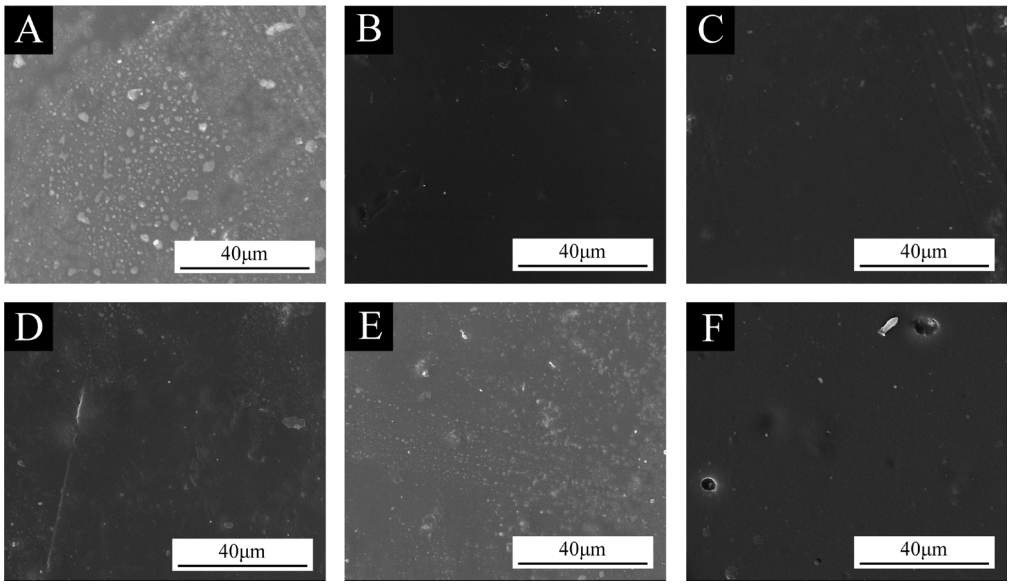


**Figure 4.** SEM images of waterborne coatings with different proportions of mixed microcapsules: (**A**) 1#, (**B**) 2#, (**C**) 3#, (**D**) 4#, (**E**) 5#, and (**F**) 6#.

### *3.3. Aging Resistance Performance Analysis*

It can be concluded from the above results that, on the optical properties, mechanical properties, and surface morphologies, both coatings of sample 1# "type A + type B" and sample 3# "type A + type B + type C" differ little from the waterborne coating containing the best microcapsule type B. In the aging test, samples 1# and 3# were selected and compared with the waterborne coating containing microcapsules of type B. The prepared coating samples with microcapsules of sample 1#, sample 3#, and the single RHP content of 5.5% were divided into three groups and placed in different environments, including the oven at 120 °C, the oven at 160 °C, and a UV climate resistance test chamber, and the surface morphologies of the waterborne coatings were observed after the climate and aging resistance tests.

#### 3.3.1. Chromatism

As shown in Figure 5, in an oven at 120 °C, from 8 h to 40 h, the chromatism of the coating containing microcapsules of "type A + type B" increased from 3.92 to 6.57. However, the chromatism of the coating containing microcapsules of "type A + type B + type C" increased from 3.07 to 3.79. Meanwhile, the chromatism of the coating containing microcapsules of type B increased from 2.77 to 2.94. On the other hand, as shown in Figure 6, in an oven at 160 °C, from 8 h to 40 h, the chromatism of the coating containing microcapsules of "type A + type B" increased from 23.80 to 38.18, the chromatism of the coating containing microcapsules of "type A + type B + type C" increased from 19.31 to 34.29, and the chromatism of the coating containing microcapsules of type B increased from 19.70 to 30.51, respectively.

Figure 7 shows the results of the UV climate resistance test. In the UV climate resistance test chamber, from 40 h to 200 h, the chromatism of the coating containing microcapsules of "type A + type B" increased from 2.20 to 5.25 from 40 h to 200 h, the chromatism of the coating containing microcapsules of "type A + type B + type C" increased from 2.05 to 4.19, and the chromatism of the coating containing microcapsules of type B increased from 3.25 to 6.92, respectively.

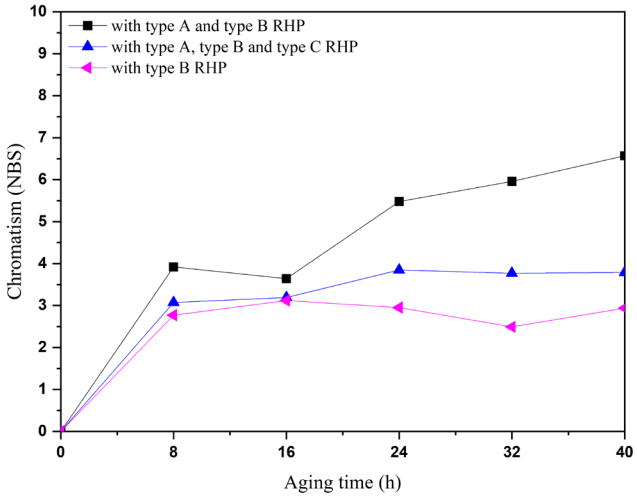


**Figure 5.** Effect of aging time on the chromatism of samples 1#, 3#, and 5# under a 120 °C aging environment.

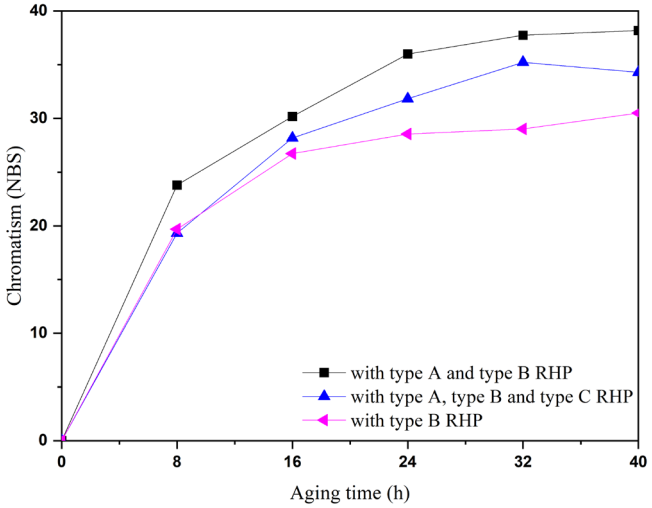


**Figure 6.** Effect of aging time on the chromatism of samples 1#, 3#, and 5# under a 160 °C aging environment.

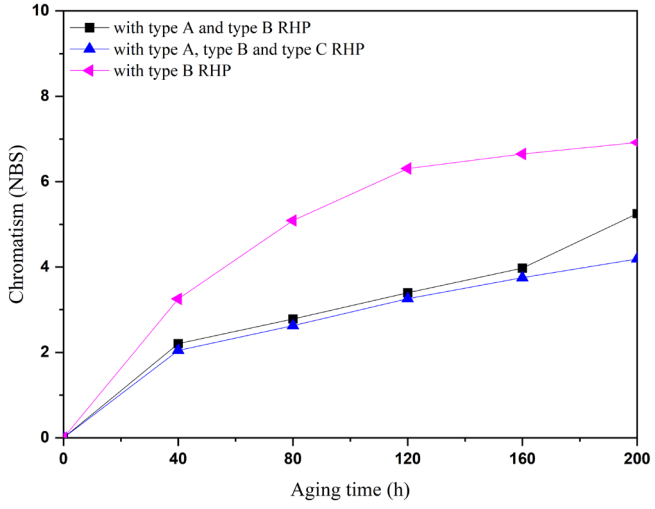


**Figure 7.** Effect of aging time on the chromatism of samples 1#, 3#, and 5# under the UV aging test.

Figures 5–7 show that, with increasing aging time, the chromatism of all of the coatings progressively intensifies. In the oven aging environment at 120 °C, the chromatism of the coating with single microcapsules (type B) showed the smallest change. For the coating with mixed microcapsules "type A + type B + type C", it showed a similar result to the coating with the single microcapsules in the first 16 h for the chromatism. Although its chromatism became larger after 16 h, the change was similar and stable. In the oven aging environment at 160 °C, the chromatism of the coatings with the two kinds of mixed microcapsules and the single microcapsules showed an obvious change, but the change values of the three samples were not much different. This is because the color of the board surface changed as a result of the carbonization of the Basswood board itself at a high temperature. In the aging environment of the UV climate resistance test chamber, the chromatism of the coatings with two mixed microcapsules was smaller than that of the coating with single microcapsules. The UV climate resistance test chamber had little impact on the Basswood substrate and should not cause the discoloration of the wood. The different microcapsules in coatings can be gradually broken during the aging process to achieve anti-aging repair. Therefore, the coating containing the mixed microcapsules performed better in the chromatism test than the coating containing the microcapsules with a single content of RHP. According to Figure 7, it is noteworthy that the chromatism of the coating containing microcapsules "type A + type B + type C" increased slowly and smoothly from 40 h to 200 h, while the chromatism of the coating added with microcapsules "type A + type B" increased drastically after 160 h. It can be judged that the chromatism of the coating increased because of the failure of all of the microcapsules in the coating in the later stage of aging.

#### 3.3.2. LLR

The LLR at an incident angle of 60° was calculated as the reference data. In an oven at 120 °C, according to Figure 8, the LLR of the coating with microcapsules of "type A + type B" reached 4.16% after 40 h, the LLR of the coating with microcapsules of "type A + type B + type C" reached 2.18%, and the LLR of the coating with microcapsules of type B reached 2.13%. This shows that the gloss of the coating does not decrease too much after aging at 120 °C. In the 160 °C ovens, as shown in Figure 9, the LLR of the coating with microcapsules of "type A + type B" reached 19.07% after 40 h, the LLR of the coating with microcapsules of "type A + type B + type C" reached 15.78%, and the LLR of the coating with microcapsules of type B reached 16.63%. In the UV climate resistance test chamber, as shown in Figure 10, the LLR of the coating with microcapsules of "type A + type B" reached 5.13% after 200 h, the LLR of the coating with microcapsules of "type A + type B + type C" reached 2.91%, and the LLR of the coating with microcapsules of type B reached 3.80%. The results demonstrate that the LLR of the coating and the aging time are positively correlated.

The aging resistance of the coatings with mixed microcapsules in different proportions was compared with that of coatings with single microcapsules. The results showed that, under the same optical and mechanical properties, the coating with mixed microcapsules of "type A + type B + type C" achieved a better duration on aging resistance than coatings with single microcapsules. After the aging test, it possessed better optical performance than that with single microcapsules and performed better on the overall performance than that with the mixed microcapsules of "type A + type B".

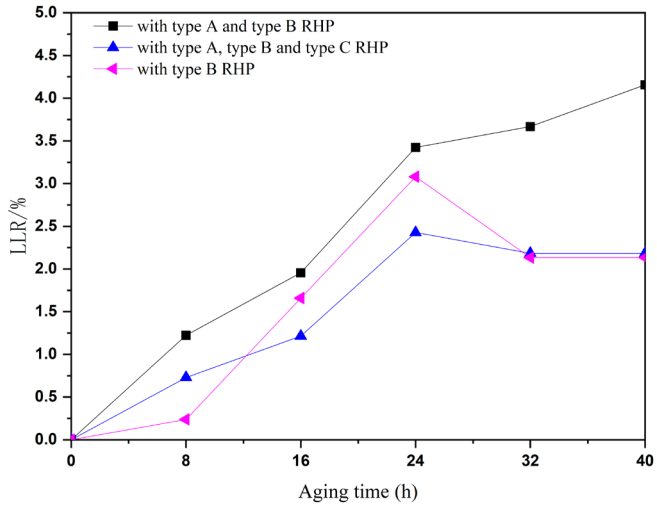


**Figure 8.** Effect of the aging time on the LLR of samples 1#, 3#, and 5# under a 120 °C aging environment.

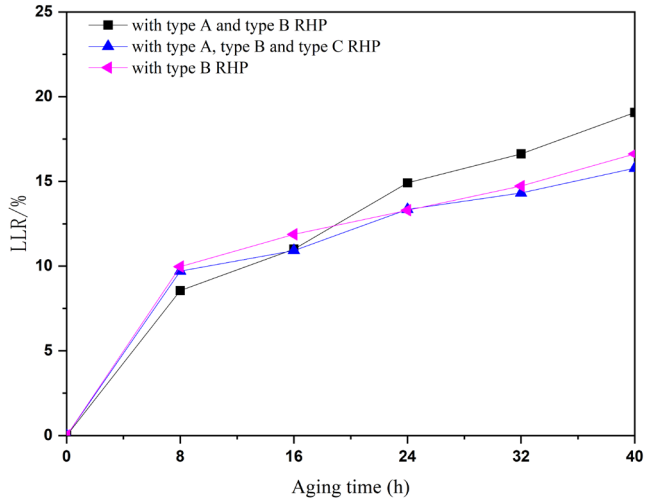


**Figure 9.** Effect of the aging time on the LLR of samples 1#, 3#, and 5# under a 160 °C aging environment.

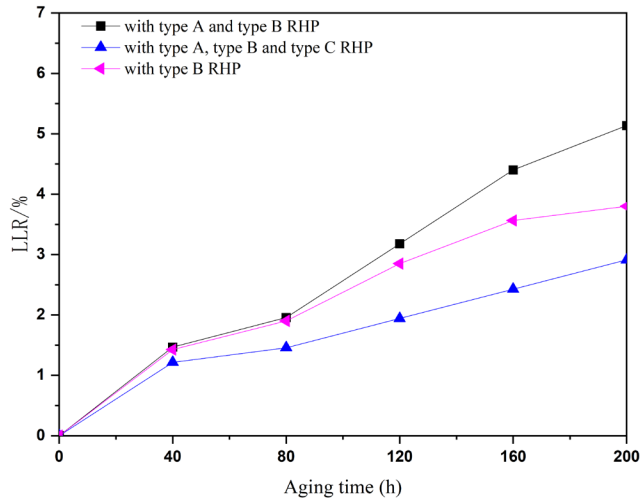


**Figure 10.** Effect of the aging time on the LLR of samples 1#, 3#, and 5# under the UV aging test.

3.3.3. Microstructure

Figures 11–13 show the SEM images of three coatings, namely, containing microcapsules "type A + type B", "type A + type B + type C", and type B after the aging test (120 °C and 160 °C) and UV weathering test. The compared SEM images before aging are shown in Figure 4A,C,D. It can be observed from Figure 11 that, after aging in an oven at 120 °C, no obvious cracks appeared on the surface of all three coatings, but the coating surface containing the mixed microcapsules of "type A + type B" showed many bubbles and protrusions. The reason can be considered due to the increase in LLR after aging. The coating containing microcapsules "type A + type B + type C" and type B only showed small cracks. Because most of the other parts are relatively smooth, the increase in the LLR is small. After aging in an oven at 160 °C (Figure 12), three kinds of coatings possessed relatively obvious cracks and bubbles. This indicates that the three coatings have substantially similar aging resistance at this temperature. From the SEM images of the UV weathering test chamber in Figure 13, for the coatings with "type A + type B" microcapsules and that with type B microcapsules, both of the coating surfaces were damaged. The amount of damage to the mixed microcapsule coating is greater than that of the single microcapsule coating. Compared with others, there was no obvious damage on the surface of the coatings containing microcapsules "type A + type B + type C". In summary, the SEM observation results were consistent with the gloss analysis results. The waterborne coating with the mixed microcapsule exhibited notably enhanced anti-aging properties during heat aging or UV aging, and maintained its integrity more effectively after the aging tests. The coating containing microcapsules of "type A + type B + type C" had the best performance.

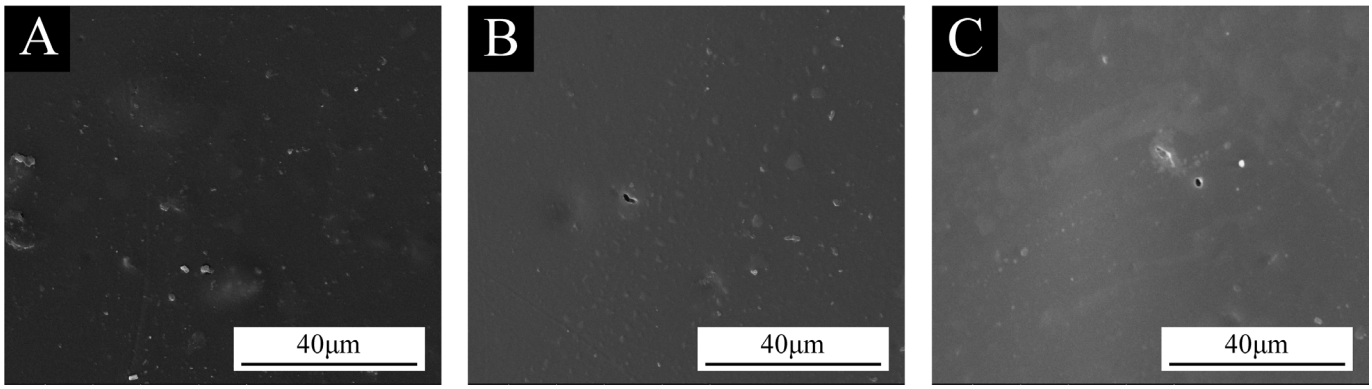


**Figure 11.** SEM images of (**A**) 1#, (**B**) 3#, (**C**) 5# after 120 °C aging test.

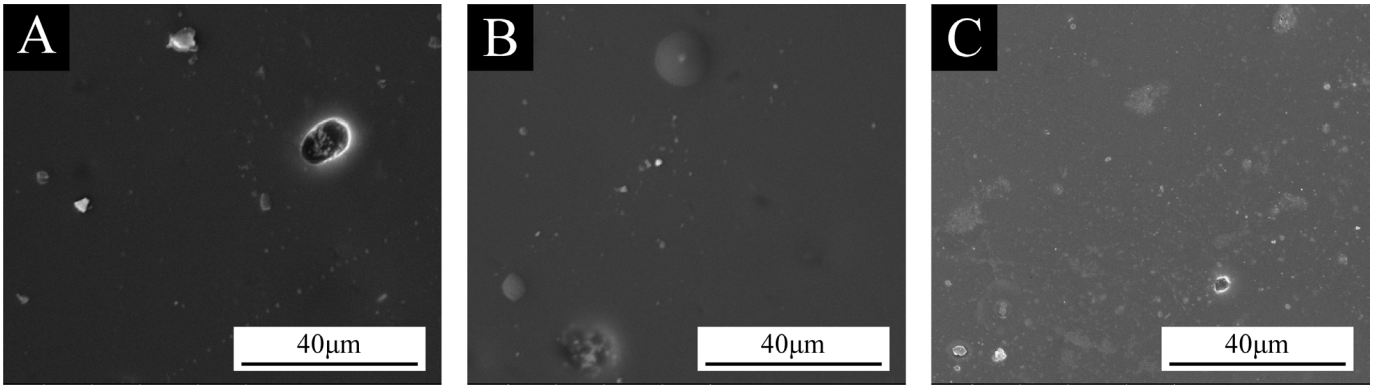


**Figure 12.** SEM images of (**A**) 1#, (**B**) 3#, (**C**) 5# after 160 °C aging test.

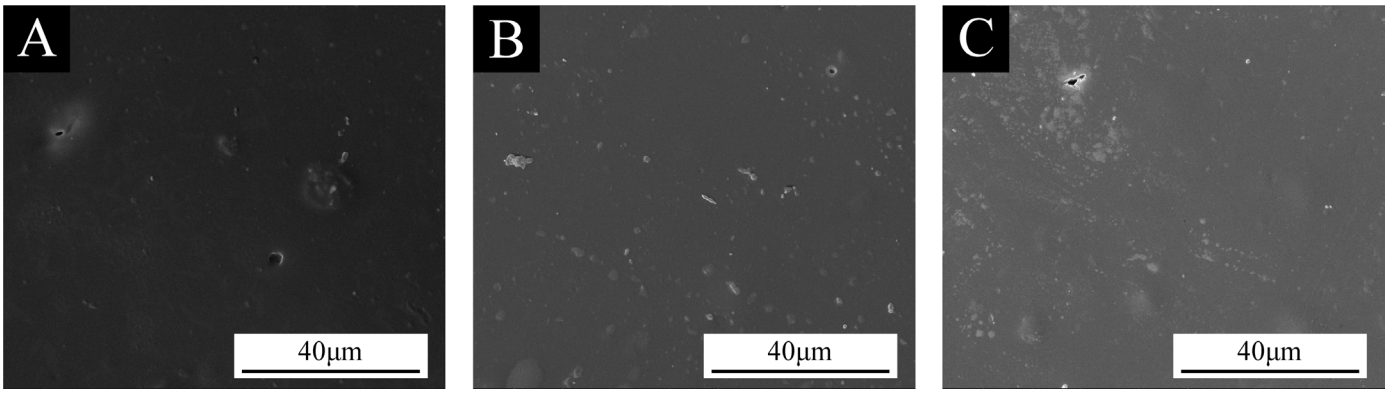


**Figure 13.** SEM images of (**A**) 1#, (**B**) 3#, and (**C**) 5# after the UV aging test.

#### 3.3.4. Infrared Spectrum Analysis

Figure 14 illustrates the infrared spectra of the coating containing microcapsules "type A + type B" before and after aging. The peaks at 2943 $cm^{-1}$ and 2875 $cm^{-1}$ belonged to methyl and methylene characteristic absorption, respectively. The absorption peak at 1731 $cm^{-1}$ was the C=O stretching vibration peak [46]. The carbon and oxygen in the ester group at 1166 $cm^{-1}$ was the characteristic absorption peak of a single bond. After the coating aging test, there was no change in the vibration absorption peak, implying that the coating did not undergo chemical reaction during the aging process, and the coating performance was stable. Figure 15 shows the infrared spectra of the coating containing microcapsules "type A + type B + type C" before and after aging. No peaks disappeared or new peaks appeared after the aging. The aging test results have shown that different aging environments have little effect on the coating composition of different mixed microcapsules.

### *3.4. Self-Healing Performance Analysis*

It can be observed from the above results that the optical properties and microscopic morphologies of the microcapsule-containing coatings with "type A + type B + type C" are similar to those of the single-proportion microcapsule coating. In addition, the microcapsule coating containing "type A + type B + type C" also performed well in mechanical properties and had better anti-aging properties. Therefore, scratch tests were performed on coatings containing microcapsules of "type A + type B + type C" to verify the effect of RHP mixed with microcapsules on the self-healing ability.

The scratched coating was placed in a normal environment, and the changes in the crack size were observed for 1 day, 3 days, 7 days, and 14 days. Figure 16 illustrates the microstructure of the scratched coating containing microcapsules "type A + type B + type C". The scratch size was 32.88 μm on day 1, 23.53 μm on day 3, 19.36 μm on day 7, and 20.74 μm on day 14, respectively. The best self-healing rate of the coating was 41.11% on the $7^{th}$ day. For the sample with single microcapsules [35], the self-healing rate was high after 7 days, at 33.4%, and the crack size decreased from 30.67 μm to 20.42 μm on day 7. In contrast, the mixed microcapsules had a higher self-healing rate than the single microcapsules. Due to the mixing of microcapsules with different toughness in the coating, when cracks occur, the microcapsules will not be completely broken, but gradually broken, which has a significant impact on the cracks and lasts for a long time. The scratch test results show that, by mixing three types of microcapsules, the self-healing performance can achieve maximization. The microcapsule coating containing "type A + type B + type C" has better stability and longer-lasting self-healing ability.

Zhu et al. [47] modified CIP and CNT materials with microcapsules and mixed them to prepare the waterborne coating with both self-healing and electromagnetic absorption functions. The coating can be applied to wood materials with a self-healing rate of 33.9%. Zou et al. [48] prepared a self-healing UV topcoat coating by in situ polymerization using UV topcoat coating microcapsules of 6.0%, with a self-healing rate of 27.32%. Compared

with these two coatings, the self-healing rate of the waterborne coating with microcapsules mixed with different RHP contents was 41.11%, indicating a strong self-healing ability and sustained effect.

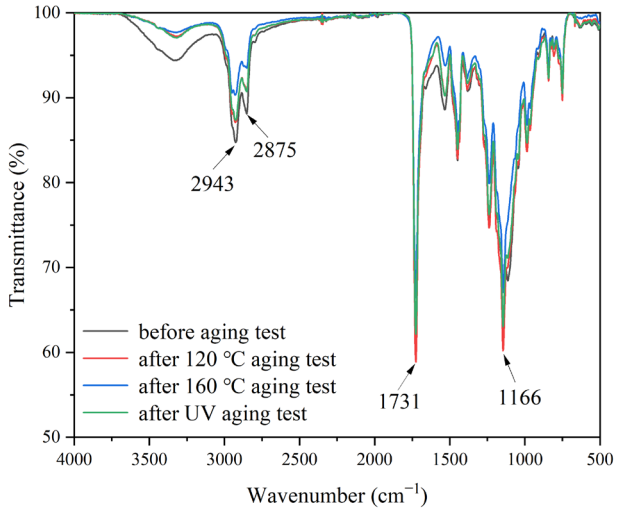


**Figure 14.** Infrared spectrum of the sample 1# (mixed microcapsules "type A + type B") coating film before and after the aging test.

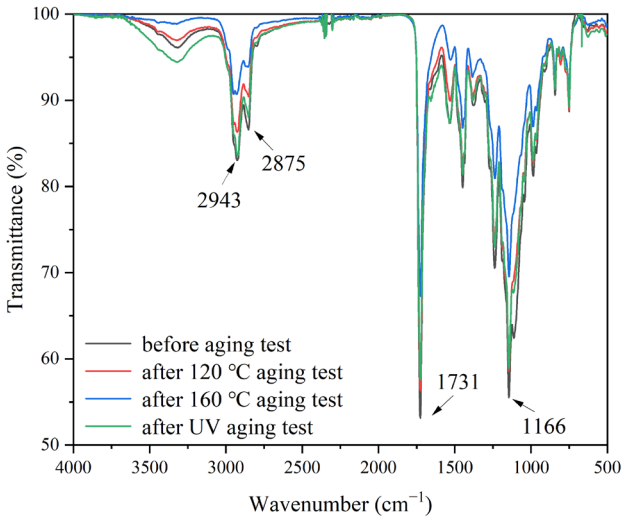


**Figure 15.** Infrared spectrum of the sample 3# (mixed microcapsules "type A + type B + type C") coating film before and after the aging test.

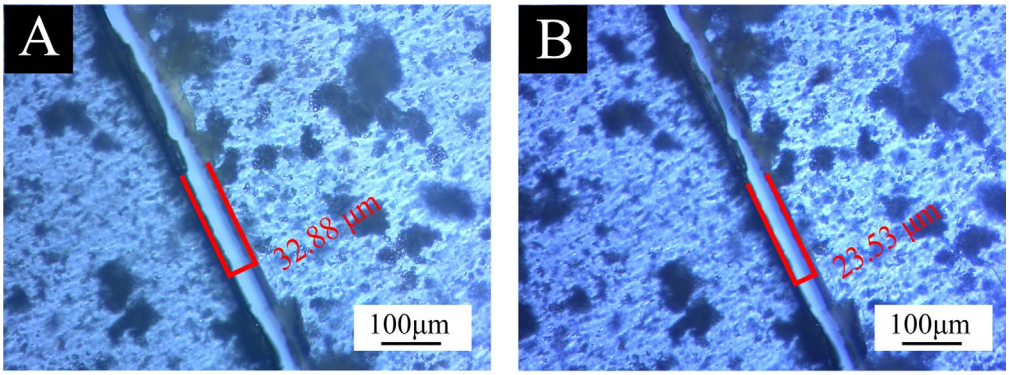


**Figure 16.** *Cont.*

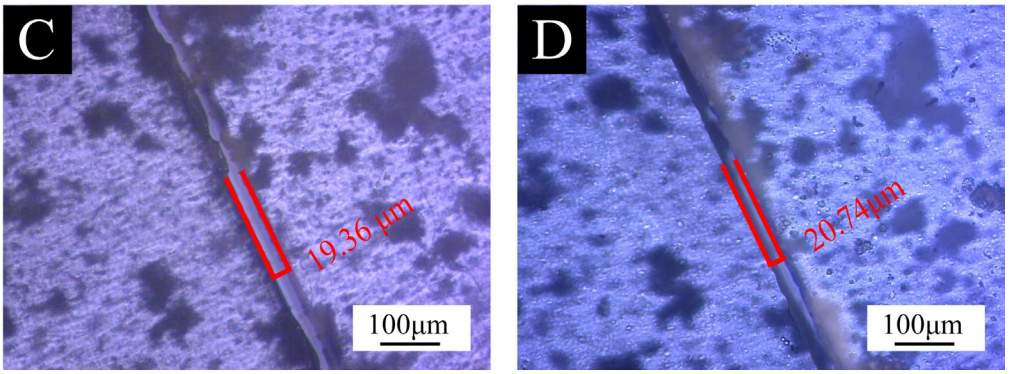


**Figure 16.** OM of the sample 3# (mixed microcapsules "type A + type B + type C") coating film after self-healing: (**A**) the 1st day, (**B**) the 3rd day, (**C**) the 7th day, and (**D**) the 14th day.

### *3.5. Roughness Test of Waterborne Coating with Mixed Microcapsules*

Considering the different sizes of the microcapsules with different RHP contents, the surface roughness test of the waterborne coatings mixed with microcapsules was required. The roughness test results showed that the surface roughness of the waterborne coating with the mixed microcapsules was 0.974 μm, while the surface roughness of that with the single optimal microcapsules was 0.936 μm. Compared with the single optimal microcapsule sample, the roughness of the mixed microcapsule sample was slightly worse, which was increased by 0.038 μm. This shows that the uniformity of the microcapsule size has a certain influence on the roughness of the coating.

However, under optimized coating process conditions, the topcoat without microcapsules can effectively cover the primer coating with mixed microcapsules. Therefore, the roughness does not change much, and the surface of the waterborne coating is relatively smooth.

## 4. Conclusions

The coatings containing the three mixed microcapsules had similar optical properties and good mechanical properties. The mixed microcapsule coating of "type A + type B + type C" exhibited the best optical and mechanical properties among all of the samples, with a chromatism of 1.10, an adhesion of zero, a hardness of 4H, an impact resistance of 7 kg·cm, and an elongation at break of 35.28%, respectively. The coating samples with the better comprehensive performance of "type A + type B" and "type A + type B + type C" were selected to compare with the coating containing the single microcapsule type B on the aging resistance and the roughness test. The results showed that the coating with mixed microcapsules containing "type A + type B + type C" had a longer repair validity period and a smoother surface. Scratch testing showed that this mixed microcapsule coating also had longer self-healing properties than a single microcapsule coating. The use of mixed RHP microcapsules for a waterborne coating on a Basswood surface provides a scientific basis for self-healing and aging resistance of multifunctional coatings.

**Author Contributions:** Conceptualization, methodology, validation, data management, and supervision, L.X.; writing—review and editing, Y.H.; resources, T.Y.; formal analysis, Y.Z.; investigation, X.Y. and J.L. All authors have read and agreed to the published version of the manuscript.

**Funding:** This project was partly supported by the Innovation and Entrepreneurship Training Program for College Students in Jiangsu Province (202410298082Z) and the Natural Science Foundation of Jiangsu Province (BK20201386).

**Institutional Review Board Statement:** Not applicable.

**Informed Consent Statement:** Not applicable.

**Data Availability Statement:** Data are contained within this article.

**Conflicts of Interest:** The authors declare no conflicts of interest.

## References


1. Li, X.L.; Zhang, M.; Yang, L.J.; Yue, X.Y.; Xiong, X.Q. Current state and development trend of China's customized home furnishing industry. *Wood Mater. Sci. Eng.* **2024**. [CrossRef]
2. Yue, X.Y.; Xiong, X.Q.; Xu, X.T.; Zhang, M. Big data for furniture intelligent manufacturing: Conceptual framework, technologies, applications, and challenges. *Int. J. Adv. Manuf. Technol.* **2024**, *132*, 5231–5247. [CrossRef]
3. Wang, G.K.; Xiong, X.Q.; Ma, Y.; Xu, X.T. Application of a digital twin model in the packaging process of the panel furniture industry. *For. Prod. J.* **2024**, *74*, 98–106. [CrossRef]
4. Zhou, C.; Huang, T.; Luo, X.; Kaner, J. Reorganisation and construction of an age-friendly smart recreational home system: Based on function capability match methodology. *Appl. Sci.* **2023**, *13*, 9783. [CrossRef]
5. Panzarasa, G.; Burgert, I. Designing functional wood materials for novel engineering applications. *Holzforschung* **2022**, *76*, 211–222. [CrossRef]
6. Liang, H.S.; Wu, Z.H.; Du, S.J. Study on the impact of environmental awareness, health consciousness, and individual basic conditions on the consumption intention of green furniture. *Sustain. Futures* **2024**, *8*, 100245. [CrossRef]
7. Luo, Z.Y.; Xu, W.; Wu, S.S. Performances of green velvet material (PLON) used in upholstered furniture. *Bioresources* **2023**, *18*, 5108–5119. [CrossRef]
8. Weng, M.Y.; Zhu, Y.T.; Mao, W.G.; Zhou, J.C.; Xu, W. Nano-silica/urea-formaldehyde resin-modified fast-growing lumber performance study. *Forests* **2023**, *14*, 1440. [CrossRef]
9. Luo, Y.R.; Xu, W. Optimization of panel furniture plates rework based on intelligent manufacturing. *Bioresources* **2023**, *18*, 5198–5208. [CrossRef]
10. Qi, Y.Q.; Zhang, Z.Q.; Sun, Y.; Shen, L.M.; Han, J.L. Study on the process optimization of peanut coat pigment staining of poplar wood. *Forests* **2024**, *15*, 504. [CrossRef]
11. Hu, W.; Liu, N.; Xu, L.; Guan, H. Study on cold/warm sensation of materials used in desktop of furniture. *Wood Res.* **2020**, *65*, 497–506. [CrossRef]
12. Chen, Y.T.; Sun, C.S.; Ren, Z.R.; Na, B. Review of the current state of application of wood defect recognition technology. *BioResources* **2023**, *18*, 2288–2302. [CrossRef]
13. Wang, C.; Zhang, C.Y.; Ding, K.Q.; Jiang, M.H. Immersion polishing post-treatment of PLA 3D printed formed parts on its surface and mechanical performance. *BioResources* **2023**, *18*, 7995–8006. [CrossRef]
14. Hu, W.; Wan, H. Comparative study on weathering durability properties of phenol formaldehyde resin modified sweetgum and southern pine specimens. *Maderas-Cienc. Tecnol.* **2022**, *24*, 17. [CrossRef]
15. Durmaz, S.; Ozgenc, O.; Avci, E.; Boyaci, I.H. Weathering performance of waterborne acrylic coating systems on flat-pressed wood-plastic composites. *J. Appl. Polym. Sci.* **2020**, *137*, 48518. [CrossRef]
16. Liu, Y.; Wu, Z. Fabrication of coatings with structural color on a wood surface. *Coatings* **2020**, *10*, 32. [CrossRef]
17. Sang, R.J.; Yang, F. Effect of $TiO_2$@$CaCO_3$ waterborne primer on the coloring performance of inkjet-printed wood product coatings. *Coatings* **2023**, *13*, 2071. [CrossRef]
18. Chang, Y.J.; Wu, Z.H. Synthesized high performance UV-cured wood wax oil using Irgacure 2959 modified thistle oil and linseed oil. *Ind. Crop. Prod.* **2024**, *218*, 118952. [CrossRef]
19. Zhu, J.; Wu, Z.; Xiong, D.; Pan, L.; Liu, Y. Preparation and properties of a novel low crystallinity cross-linked network waterborne polyurethane for water-based ink. *Prog. Org. Coat.* **2019**, *133*, 161–168. [CrossRef]
20. Agnol, L.D.; Dias, Z.; Yan, F.T.G.; Ornaghi, H.L.; Sangermano, M.; Bianchi, O. UV-curable waterborne polyurethane coatings: A state-of-the-art and recent advances review. *Prog. Org. Coat.* **2021**, *154*, 106156. [CrossRef]
21. Liu, Q.Q.; Gao, D.; Xu, W. Effect of paint process on the performance of modified poplar wood antique. *Coatings* **2021**, *11*, 1174. [CrossRef]
22. Ling, K.L.; Feng, Q.M.; Huang, Y.H.; Li, F.; Huang, Q.F.; Zhang, W.; Wang, X.C. Effect of modified acrylic water-based paint on the properties of paint film. *Spectrosc. Spect. Anal.* **2020**, *40*, 2133–2137.
23. Zhang, H.Q.; Feng, X.H.; Wu, Y.; Wu, Z.H. Factors influencing the properties of UV-cured self-matting film. *Prog. Org. Coat.* **2024**, *189*, 108241. [CrossRef]
24. Li, H.Y.; Cui, Y.X.; Li, Z.K.; Zhu, Y.J.; Wang, H.Y. Fabrication of microcapsules containing dual-functional tung oil and properties suitable for self-healing and self-lubricating coatings. *Prog. Org. Coat.* **2018**, *115*, 164–171. [CrossRef]
25. Song, Y.; Chen, K.F.; Wang, J.J.; Liu, Y.; Qi, T.; Li, G.L. Synthesis of polyurethane/poly(urea-formaldehyde) double-shelled microcapsules for self-healing anticorrosion coatings. *Chin. J. Polym. Sci.* **2020**, *38*, 45–52. [CrossRef]
26. Tezel, O.; Cigil, A.B.; Kahraman, M.V. Dual microcapsules based epoxy/polyethyleneimine autonomous self-healing system for photo-curable coating. *Polym. Advan. Technol.* **2021**, *32*, 553–563. [CrossRef]
27. Uzoma, P.C.; Liu, F.C.; Han, E.H. Multi-stimuli-triggered and self-repairable fluorocarbon organic coatings with urea-formaldehyde microcapsules filled with fluorosilane. *J. Mater. Sci. Technol.* **2020**, *45*, 70–83. [CrossRef]
28. Bar, H.; Bianco-Peled, H. The unique nanostructure of shellac films. *Prog. Org. Coat.* **2021**, *157*, 106328. [CrossRef]
29. Patel, A.R.; Remijn, C.; Cabero, A.I.M.; Heussen, P.C.M.; Hoorn, J.W.M.S.; Velikov, K.P. Novel all-natural microcapsules from gelatin and shellac for biorelated applications. *Adv. Funct. Mater.* **2013**, *23*, 4710–4718. [CrossRef]
30. Weththimuni, M.L.; Milanese, C.; Licchelli, M.; Malagodi, M. Improving the protective properties of shellac-based varnishes by functionalized nanoparticles. *Coatings* **2021**, *11*, 419. [CrossRef]

31. Naikwadi, A.T.; Samui, A.B.; Mahanwar, P.A. Melamine-formaldehyde microencapsulated n-Tetracosane phase change material for solar thermal energy storage in coating. *Sol. Energ. Mat. Sol. C* **2020**, *215*, 110676. [CrossRef]
32. Satdive, A.; Mestry, S.; Patil, D.; Mhaske, S.T. Synthesis of melamine formaldehyde cured castor oil based hydroxyl functional alkyd for coating application. *Prog. Org. Coat.* **2019**, *131*, 165–175. [CrossRef]
33. Liu, E.W.; Wu, Z.H. Preparation and characterization of cellulose nanofibers/polybenzoxazine–poly(vinyl alcohol) double network foam based on multiple hydrogen bond structure. *ACS Appl. Polym. Mater.* **2024**, *6*, 6219–6228. [CrossRef]
34. Yap, S.Y.; Sreekantan, S.; Hassan, M.; Sudesh, K.; Ong, M.T. Characterization and biodegradability of rice husk-filled polymer composites. *Polymers* **2021**, *13*, 104. [CrossRef] [PubMed]
35. Yan, X.X.; Han, Y.; Yin, T.Y. Coating process optimization and self-healing performance evaluation of shellac microcapsules coated with melamine/rice husk powder. *Appl. Sci.* **2021**, *11*, 8373. [CrossRef]
36. Yan, X.X.; Han, Y.; Yin, T.Y. Synthesis of urea-formaldehyde microcapsule containing fluororesin and its effect on performances of waterborne coatings on wood surface. *Polymers* **2021**, *13*, 1674. [CrossRef] [PubMed]
37. Yan, X.X.; Wang, L. Preparation of shellac resin microcapsules coated with urea formaldehyde resin and properties of waterborne paint films for Tilia amurensis Rupr. *Membranes* **2020**, *10*, 278. [CrossRef] [PubMed]
38. Li, W.B.; Yan, X.X. Effects of shellac self-repairing and carbonyl iron powder microcapsules on the properties of Dulux waterborne coatings on wood. *Polymers* **2023**, *15*, 2016. [CrossRef] [PubMed]
39. *GB/T 4893.6-2013*; Test of Surface Coatings of Furniture-Part 6: Determination of Gloss Value. Standardization Administration of the People's Republic of China: Beijing, China, 2013.
40. *GB/T 6739-2022*; Paints and Varnishes-Determination of Film Hardness by Pencil Test. Standardization Administration of the People's Republic of China: Beijing, China, 2022.
41. *GB/T 4893.4-2013*; Test of Surface Coatings of Furniture-Part 4: Determination of Adhesion—Cross Cut. Standardization Administration of the People's Republic of China: Beijing, China, 2013.
42. *GB/T 1732-2020*; Determination of Impact Resistance of Coating Films. Standardization Administration of the People's Republic of China: Beijing, China, 2020.
43. *BS EN 15977-2011*; Rubber or plastic coated fabrics. Mechanical properties. Determination of the elongation under load and the residual deformation. British Standards Institution: London, UK, 2011.
44. Hu, W.G.; Yu, R.Z. Study on the strength mechanism of the wooden round-end mortise-and-tenon joint using the digital image correlation method. *Holzforschung* **2024**. [CrossRef]
45. Hu, W.G.; Luo, M.Y.; Yu, R.Z.; Zhao, Y. Effects of the selected factors on cyclic load performance of T-shaped mortise-and-tenon furniture joints. *Wood Mater. Sci. Eng.* **2024**. [CrossRef]
46. Zhao, B.B.; Jiao, C.L.; He, W.; Ma, Y.X.; Sun, S.X.; Du, W.H.; Cheng, Y. Optimization of the branched structure to enhance the corrosion protection of waterborne acrylic-alkyd resins on iron-based materials. *Prog. Org. Coat.* **2024**, *194*, 108568. [CrossRef]
47. Zhu, Y.; Li, W.B.; Yan, X.X. Effect of Blending of Shellac, Carbonyl Iron Powder, and Carbonyl Iron Powder/Carbon Nanotube Microcapsules on the Properties of Coatings. *Coatings* **2024**, *14*, 75. [CrossRef]
48. Zou, Y.M.; Xia, Y.X.; Yan, X.X. Effect of UV Top Coating Microcapsules on the Coating Properties of Fiberboard Surfaces. *Polymers* **2024**, *16*, 2098. [CrossRef] [PubMed]